

BASIC SCIENCE ARTICLE OPEN ACCESS

Simple Characterization of Cylindrical Diffuser Fibers With a Fluorescent Layer

Herbert Stepp  | Ronald Sroka 

Laser-Forschungslabor, LIFE Center, University Hospital, LMU Munich, Planegg, Germany

Correspondence: Herbert Stepp (herbert.stepp@med.uni-muenchen.de)**Received:** 27 March 2024 | **Revised:** 27 May 2024 | **Accepted:** 10 June 2024**Keywords:** cylindrical diffuser fiber | intensity profile | interstitial laser thermotherapy | photodynamic therapy**ABSTRACT**

Objectives: A fast, simple, versatile, and reliable method to record light emission intensity profiles of cylindrical light diffusers (CDFs) in air and transparent liquids has been developed.

Methods: A fluorescent color glass filter (RG695) converts red light emitted by a cylindrical diffuser fiber into near-infrared light in an emission angle-independent manner. The red light was provided from a diode laser system at 635 nm. Near-infrared fluorescence from the RG695 was imaged with a camera. Images from this camera were processed to obtain emission intensity profiles. Cylindrical diffuser fiber profiles of four different manufacturers were compared.

Results: The proposed method provides angle-independent intensity profiles of cylindrical diffuser fibers with a single camera shot. It could be demonstrated that dependent on the underlying principle of how the diffuser fiber tips emit light, the emission profile can change significantly in media with different refractive indices.

Conclusions: By converting the light emitted by a diffuser fiber tip into fluorescence light one can eliminate the dependence of the recorded profile on the emission angle from the diffusor. This approach allows for easily taking into account refraction-index (mis)matching by placing the equipment into a suitable liquid. The proposed measurement principle bears potential for quality assurance measurements of CDFs used for interstitial laser thermotherapy or photodynamic therapy.

1 | Introduction

Cylindrical diffuser fibers (CDFs) are light guiding fibers equipped with a tip, which emits light sideways over a certain fiber length, in the range of one to several centimeters [1]. Usually, laser light is emitted for applications such as thermal coagulation or photodynamic therapy (PDT) of tissue. Some CDFs limit the light emission to a hemi-cylinder to shield parts of the tissue from light exposure. The inner design of such CDF laser light applicators is often proprietary and can rely on various different physical principles. A simple approach is to add some scattering material to transparent silicone in a thin transparent hose and attach it to the flat cleaved end of the light guiding fiber. A mirror at the distal end of the scattering silicone further homogenizes the light emission due to

reflection of the remaining axially transmitted light. Another approach is to make use of a light homogenizing partial integrating sphere effect by using a diffusely scattering hose material. One can also manipulate the fiber core itself to scatter light by acid roughening or by engraving defects with pulsed lasers [2–5]. With such technology and combinations of them, the radiance profile emitted along the diffusing tip can be tailored in a prescribed manner, enabling so-called conformal emission profiles [6].

CDFs are typically employed to irradiate cylindrical or spherical organ surfaces, such as esophagus [7] or urinary bladder [8] or they are used for interstitial applications such as PDT or laser-induced thermotherapy LITT of malignant brain tumors [9] or benign prostate hyperplasia and prostate cancer [10]. One of the

This is an open access article under the terms of the [Creative Commons Attribution-NonCommercial-NoDerivs](https://creativecommons.org/licenses/by-nc-nd/4.0/) License, which permits use and distribution in any medium, provided the original work is properly cited, the use is non-commercial and no modifications or adaptations are made.

© 2024 The Author(s). *Lasers in Surgery and Medicine* published by Wiley Periodicals LLC.

advantages of CDFs versus bare-end fibers is the ability to target larger tissue volumes with fewer invasive insertions. Another one is the much lower fluence rate at the light-emitting surface. The overall aim is to deliver light of a certain dose (in J/cm^2) to a target tissue volume to induce thermal or photochemical reactions. In the vast majority of cases, a homogenous light emission profile is desired, meaning that along the length of the diffusing tip the same light intensity is emitted, resulting in a so-called hat-top intensity profile along the fiber axis. To assess, how well the real emission profile matches the desired one, several measurement approaches have been suggested. A simple and quick setup just takes a picture with a camera perpendicular to the fiber axis and plots an intensity profile along the diffusing tip [11, 12]. This approach will not yield correct results, if the diffuser emits with a variable polar angle distribution along its length: the camera will only detect light entering the objective lens, that is, light emitted rather perpendicularly from the diffuser axis. In case light is emitted in a predominantly forward or backward direction from the diffuser tip, much of it will not be detected. If this changes along the length of the diffuser tip, the measured profile is not correctly indicating the relative irradiance available for the interaction with tissue. An attempt to overcome this weakness of camera profile measurements has been described by Murrer et al. [13]. Their approach is rather complex, however: Multiple detectors are evenly distributed over the entire polar angle range, all looking at the same spot on the diffuser tip. To obtain an intensity profile, the diffuser has to be scanned relative to the measurement setup along the diffuser tip length. A somewhat simpler setup is described by Vesselov et al. [2, 14]. It uses a single detector mounted in a goniometer apparatus and scans along polar and azimuth angles to cover the farfield angular emission profiles. An additional scanning is needed to measure the longitudinal profile. Other setups use a linear detector array (or 2D sensor) in close proximity of the fiber [12] or scan a bare cleaved fiber or isotropic detecting fiber tip along the diffuser with or without being immersed into a tissue mimicking phantom [15, 16].

Here, we propose a simple approach, which avoids most of the technical complexity and drawbacks of other diffuser profile measurement setups. We employ a fluorescent layer, which is imaged by a farfield camera. The fluorescent layer can be a thin flexible foil or, as used in the present investigation, a color glass

longpass filter. The optical properties of the fluorescent layer should be such that the light emitted by the diffuser tip is absorbed by a fluorophore inside the layer within a short distance and converted into fluorescence photons. The fluorescence of the layer would be emitted isotropically. The spectral band of the fluorescence, which is in the transmission range of the layer, would not encounter any absorption or scatter during travel through the layer. This is true if the fluorescence light is not reabsorbed within the layer, requiring either a large Stokes shift or the detection of wavelengths with low absorption within the layer, for example, by using a suitable longpass filter in front of the camera. The position and intensity of the fluorescence indicate location and intensity of the light emitted by the CDF, if the layer is in contact with the diffuser surface. This can be imaged by a camera and a reliable profile is easily calculated from that image. By adjusting the distance between CDF and the fluorescent layer, it can also be imaged, how the diffuser illuminates hollow organs, such as the esophagus. The setup can also be immersed in liquids, thus overcoming refractive index mismatching challenges in case of irradiation in fluid environment or interstitially in tissue.

2 | Materials and Methods

2.1 | Setup

A simple embodiment of the proposed approach is shown in Figure 1. In this case, laser light at 635 nm and a power of 34 mW was coupled into the CDF (fiber core diameters: 400 or 600 μm). In this feasibility experiment, a color glass filter was used as a fluorescent layer (RG695, 2 mm, Schott, pgo, Iserlohn). CDFs of four different manufacturers were tested: #1: diffuser tip length 30 mm, volume scatterer with distal mirror; #2: diffuser tip length 30 mm, surface scatterer, #3: diffuser tip length 30 mm, volume scatterer with distal mirror; #4: diffuser tip length 20 mm, volume scatterer, no distal mirror. These CDFs had been in use before for various laboratory applications. The color camera (DBK38UX267, The Imaging Source, Bremen, Germany), sensitive to wavelengths beyond 900 nm, was equipped with a 25 mm objective (Cosmicar, Pentax). Images were grabbed by a specific software (IC capture, version 2.4, The Imaging Source). The distance between CDF and objective lens was kept constant to be

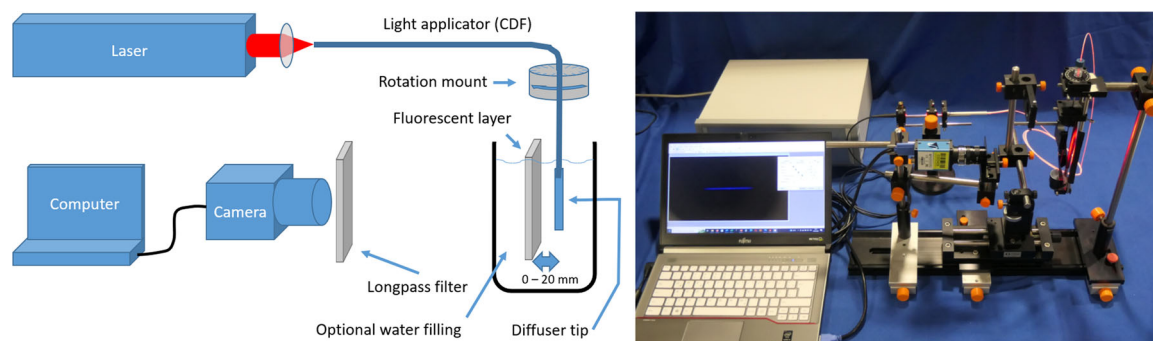


FIGURE 1 | Schematic and picture of the fluorescent layer approach. The CDF is fixed in a manual rotation mount to enable measurements at distinct azimuth angles. To guarantee a straight diffuser tip and the closest proximity to the fluorescent layer (a fluorescent color glass longpass filter, RG695, in all figures except Figure 3, right) over the entire length of the diffuser tip, the CDF is fed through a thin steel tube and the distal last 1 mm of the CDF is also held in place by another collinear similar tube.

12.5 cm. Intensity profiles were calculated using (ImageJ, Fiji, 1.53, NIH, USA). Directly in front of the objective, non-fluorescent longpass filters (RG760, 2 mm and RG800, 2 mm, Schott, pgo, Iserlohn) were positioned to block residual red light emitted by the CDF and still transmitted through the fluorescent layer (RG695 filter) close to the CDF. Filter transmission spectra (Ocean Optics USB 2000+, Iserlohn, Germany) and spectra measured at the position of the objective are shown in Figure 2. If the two longpass filters in front of the objective lens were not employed, the camera recorded exclusively red light from the CDF transmitted through the fluorescent layer, because the fluorescence intensity of that layer was so much weaker that it was not detectable by the camera at the given sensitivity setting. These images are depicted as “direct image” below. This corresponds to measuring without any filter or fluorescent layer, as is done with other techniques. Gain and integration time of the camera system were always adjusted such that overexposure of the detector was avoided.

To mimic interstitial use, the CDFs and fluorescent layer (RG695 filter) could be immersed in water (see schematic in Figure 1), thus refraction index mismatch can be eliminated to simulate interstitial applications.

2.2 | Image Recording

The images were recorded using the following camera parameters: RGB24 mode, detector: 4096×2160 pixels, gamma set to 1. In the air, the following images were recorded: 1. “Direct image” of CDF without longpass filters in front of the objective, but with fluorescent layer in place, 2. “Fluorescence image” through longpass filters and fluorescent layer with CDF in contact, 3. Fluorescence image through longpass filters and fluorescent layer with CDF in 5 mm distance from fluorescent layer, 4. Fluorescence image through longpass filters and fluorescent layer with CDF in 10 mm distance from the fluorescent layer.

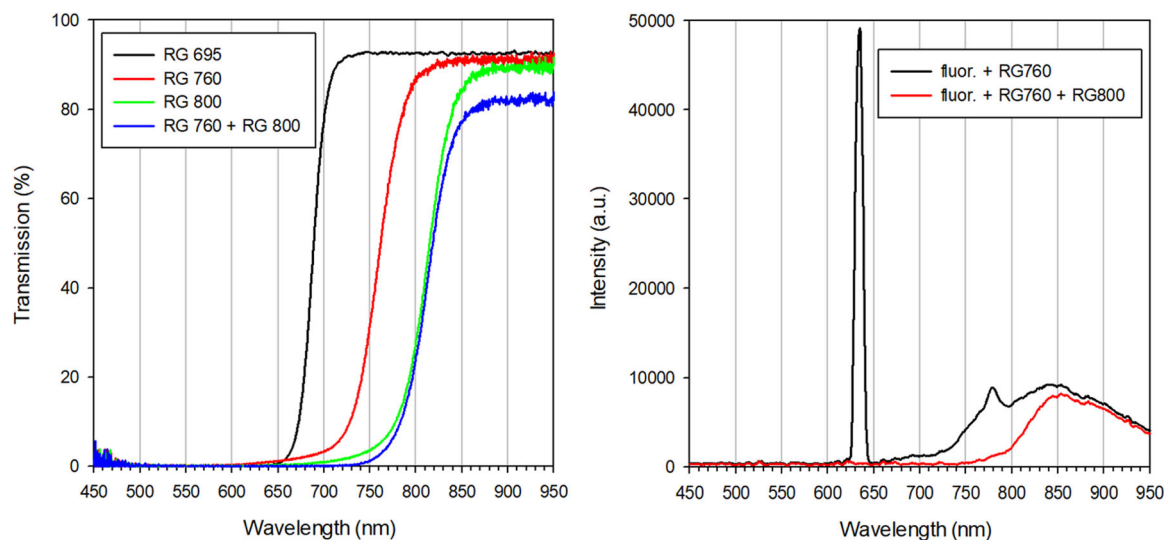


FIGURE 2 | Left: spectral filter characteristics of the longpass filters used in front of the camera (RG760 and RG800) and close to the CDF as the fluorescent layer (RG695). Right: Light detected by the camera with RG695 in the light path and either only RG760 in place (black curve) or both additional filters (red curve).

2.3 | Calculation of Intensity Profiles

Image calibration in absolute mm was performed with Image J using an image of a ruler. For shading and flatfield correction, first, the red channel of the direct or fluorescence image was selected and then divided by the red channel of an image of a sheet of white paper homogeneously illuminated with white light. A large rectangle was drawn around the imaged diffuser tip (same for all four images taken for each CDF). By means of the command “plot profile” (ImageJ), the intensity (gray value) profile covered by the rectangle was calculated. This command calculates an average intensity along a line perpendicular to the fiber axis and then plots these values along a line parallel to the fiber axis. Azimuth intensity plots of the CDFs were obtained from fluorescence images recorded at distinct rotation angles, manually adjusted with a rotation stage, where the CDF was firmly fixed in a so-called Tuohy-Borst adapter. The mean gray values of seven regions of interest, evenly distributed along the diffuser tip were plotted in a polar plot diagram (see Figure 7).

2.4 | Spatial Resolution

With the proposed method, the camera should merely detect fluorescence light excited in the fluorescent layer (RG695 filter) in front of the CDF, where the CDF diffuses excitation light into the fluorescent layer. These excitation photons will travel a short distance within the fluorescent layer before being absorbed and converted to fluorescence photons. The absorbance of this fluorescent layer was measured to be $A = 2.6$ (data not shown), which means that less than 0.25% of the red excitation light at 635 nm is transmitted through this 2 mm thick fluorescent layer, and the optical penetration depth of the excitation light is approximately $300 \mu\text{m}$. This effect will somewhat reduce the spatial resolution of the so measured CDF intensity profile depending on the angle distribution of the light emitted from the CDF surface. The spatial resolution was determined with a $50 \mu\text{m}$ core flat cut fiber positioned

perpendicularly in contact with the fluorescent layer. The camera was positioned close to the fluorescent layer to obtain a magnified fluorescence image with a resolution of ca. $2\ \mu\text{m}$ per pixel. In Figure 3 left and center, the normalized intensity profiles of the fiber surface (black curve) and the fluorescence spot excited in the fluorescent layer (red curve) are shown. Under these conditions, the resolution is still in the range of $100\ \mu\text{m}$ as can be read from Figure 3 center.

2.5 | Statistics

The reproducibility of the measurement had been assessed by repeating the placements of CDF and camera 10 times. CDF #2 was used for this measurement. The azimuth angle was tried to be reproduced by adjusting a pen-mark on the fiber at the same angle position for each measurement. The recorded intensity profiles of the fluorescence images were adjusted to set the zero position at 50% of the proximal flank of the profile. A mean profile was then calculated from all individual profiles and the residual profiles plotted in % deviation from the maximum value of the mean profile. From 0 to 30 mm the individual root mean squares and their corresponding mean and standard deviation for the 10 repetitions were calculated. This reproducibility assessment was performed using a 1 mm RG780 longpass filter as the fluorescent layer (see below).

3 | Results

The setup proved robust and allowed for rather reproducible measurements: Figure 3 right shows the intensity profiles of the fluorescence images together with the residuals from the mean profile obtained after complete removal and reinsertion of CDF #2 and readjustment of the camera. The mean root mean squares were determined as 2.3% (range 0.5% to 3.4%, standard

deviation 0.9%). Part of the recorded variations in the intensity profiles is probably contributable to not reproducing the azimuth angle perfectly.

In Figure 4 the diffuser tips of CDF #1 and #2 together with their emission profile images measured in air are shown. The corresponding intensity profiles of all four CDFs are shown in Figure 5. As mentioned, the construction of CDF #1 and #3 rely on roughly the same diffusing principle: a flat cut fiber sends light into a scattering rod, the distal end being sealed with a mirror. Additional X-ray markers are visible in some of the profiles (see blue arrows in Figure 4). Due to a rather low concentration of scatterers in the scattering rod, the diffuser tip looks rather transparent (see top left image in Figure 4). The construction of CDF #2 follows an apparently different principle. The outer surface of the diffuser tip is strongly scattering, the diffuser tip looks white (see top right image in Figure 4). The construction of CDF #4 is similar to CDFs #1 or #3, but lacks the mirror at the distal end. This has consequences for the measured intensity profiles and their differential behaviors in air versus in water. The direct image profiles of the diffuser tips of CDFs #1, #3, and #4 (black lines in Figure 5) are rather similar to the corresponding fluorescence image profiles (red lines in Figure 5), with some deviations at the ends of the diffuser tip. The similarity of direct and fluorescence profile is almost perfect for the “white” diffuser tip of CDF #2. If the fluorescent layer is 5 or 10 mm away from the diffuser tip, the profiles become significantly broader (green and blue curves in Figure 5).

In Figure 6, the CDF profiles measured in water in comparison to the ones measured in air are shown, both for the direct images (compare black and green lines) and the fluorescence images in contact with the fluorescent layer (compare red and blue lines). For CDF #1, the “center-normalized” profiles change significantly when the container is filled with water in relation to the measurement in air. In comparison, this is not

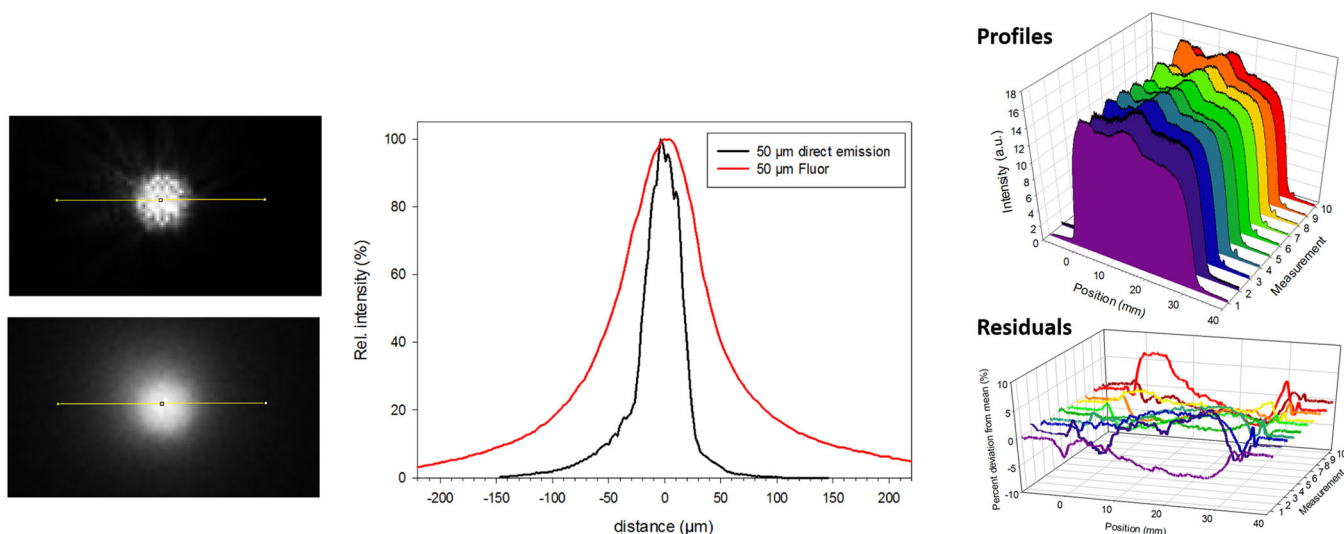


FIGURE 3 | Left: image of a $50\ \mu\text{m}$ flat cut fiber in contact with the fluorescent layer. Top left: red channel of the camera without additional longpass filters in front of the objective lens. Bottom left: NIR-fluorescence of the filter (additional longpass filters mounted in front of the objective lens). Center: normalized intensity profiles along the yellow lines in the images to the left. Right: profiles and residuals (in percent deviation from the mean profile) of 10 repetitions of CDF #2 and camera placements and adjustments in the setup.

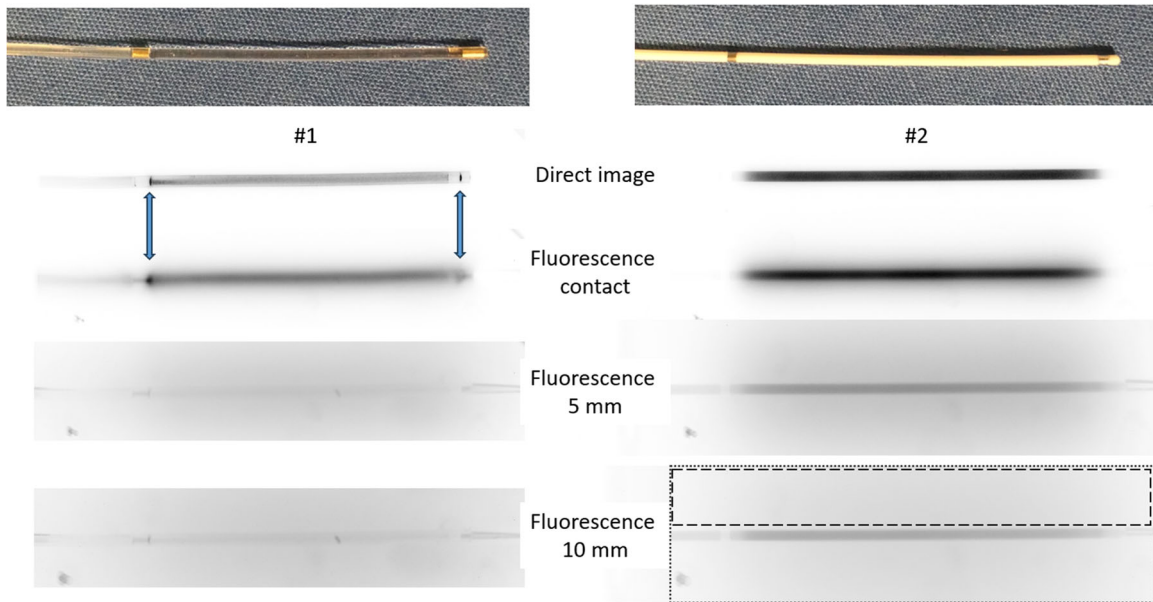


FIGURE 4 | Diffuser tips of CDF #1 and #2. From top to bottom: photograph, intensity recorded in the red channel (no longpass filters in front of the objective lens, “direct image”), fluorescence image with CDF in almost direct contact with the fluorescent layer, fluorescence image of the layer in 5 mm distance from the CDF, same in 10 mm distance. All profile images are displayed with inverted look-up-table. Blue arrows indicate influence of the X-ray markers on the recorded intensities. Dotted rectangle: Area used to calculate the profiles depicted as solid lines in Figure 5, dashed rectangle: Area used to calculate the profiles depicted as dashed lines in Figure 5.

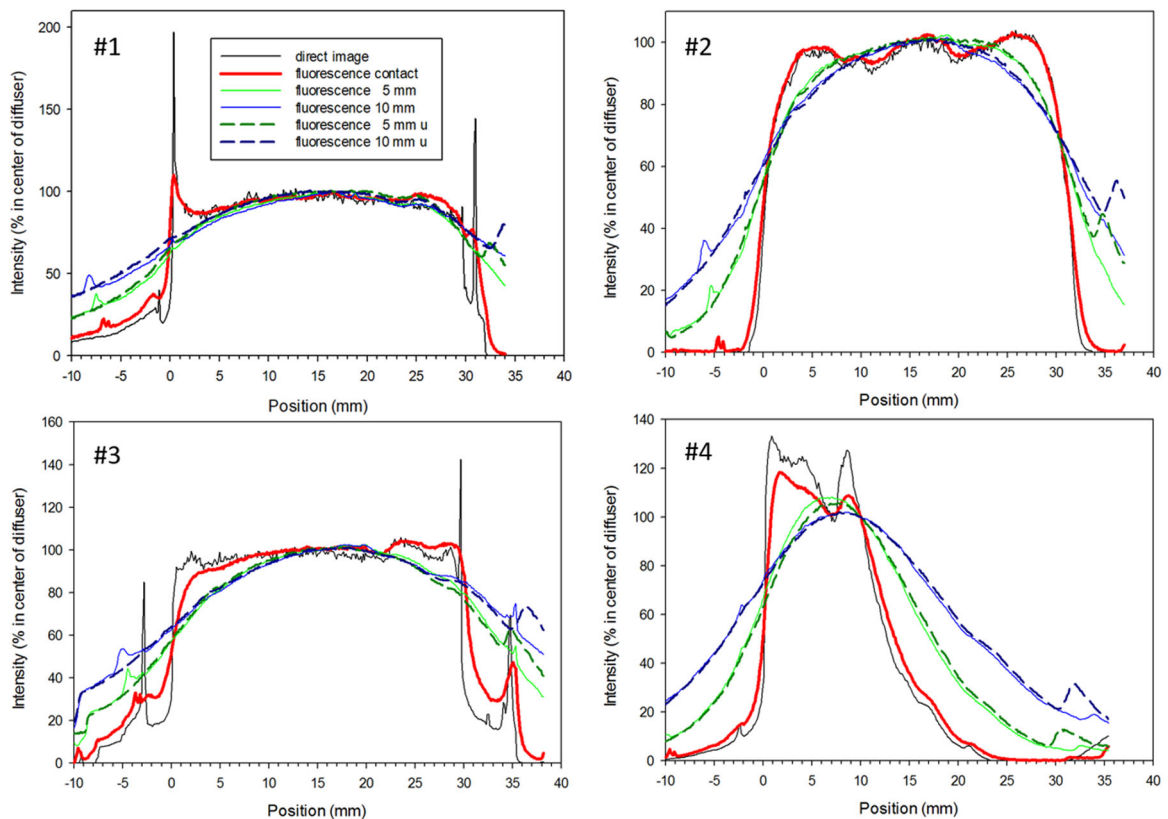


FIGURE 5 | Intensity profiles of four different CDFs. Black curves: direct image intensity profile (no longpass filters in front of the objective lens), red curves: fluorescence intensity profile with CDF in direct contact with the fluorescent layer, light green and light blue curves: fluorescence intensity profiles of the fluorescent layer in 5 and 10 mm distance from the CDF, respectively. The dashed lines (“fluorescence 5 mm u” and “fluorescence 10 mm u”) are obtained, when the rectangles for intensity profile calculation were drawn in the upper half of the profile image, sparing the image of the diffuser (as indicated in the bottom right image in Figure 4).

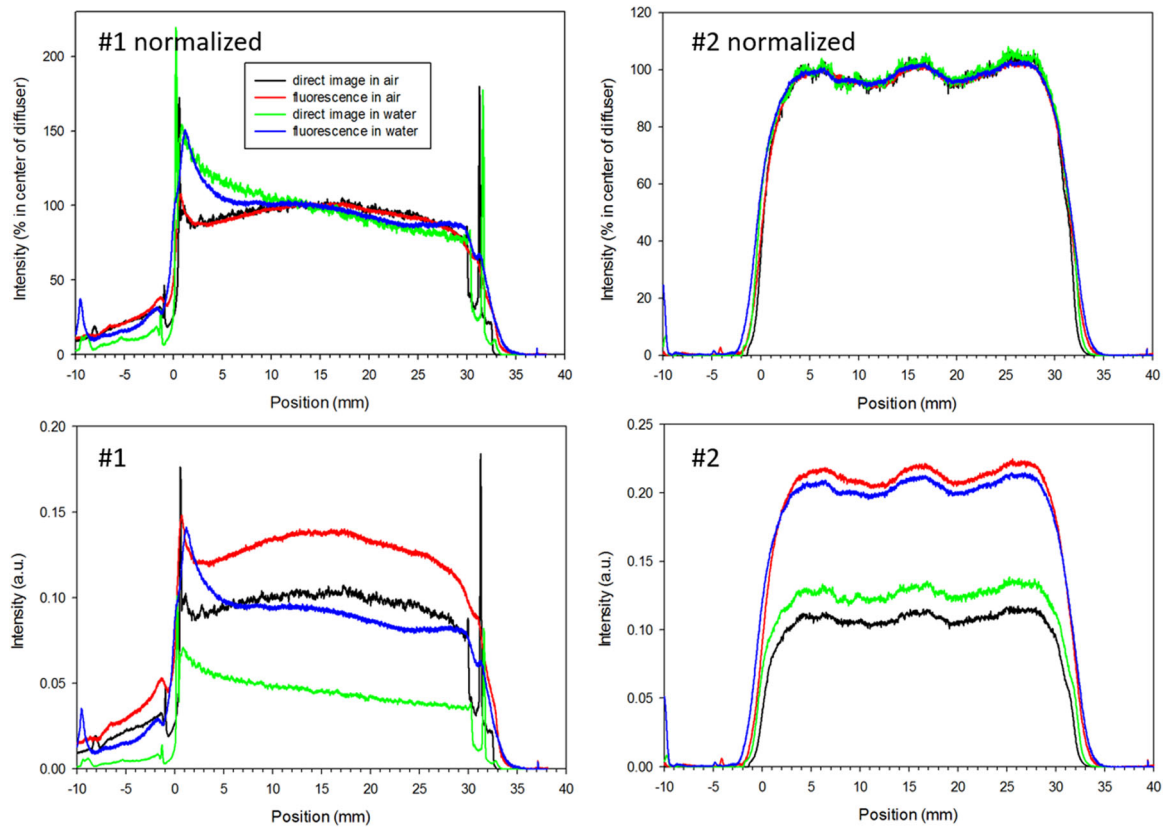


FIGURE 6 | Intensity profiles of CDFs #1 and #2 in air and in water. Black and green curves: direct image intensity profiles (no longpass filters in front of the objective lens), red and blue curves: fluorescence intensity profiles with CDF in direct contact with the fluorescent layers. Measurements were done with the CDF and fluorescent layer in a transparent empty container (air) and after filling the container with water (water). Top row: profiles normalized to the intensity in the center of the diffuser tip (15 mm), bottom row: without normalization.

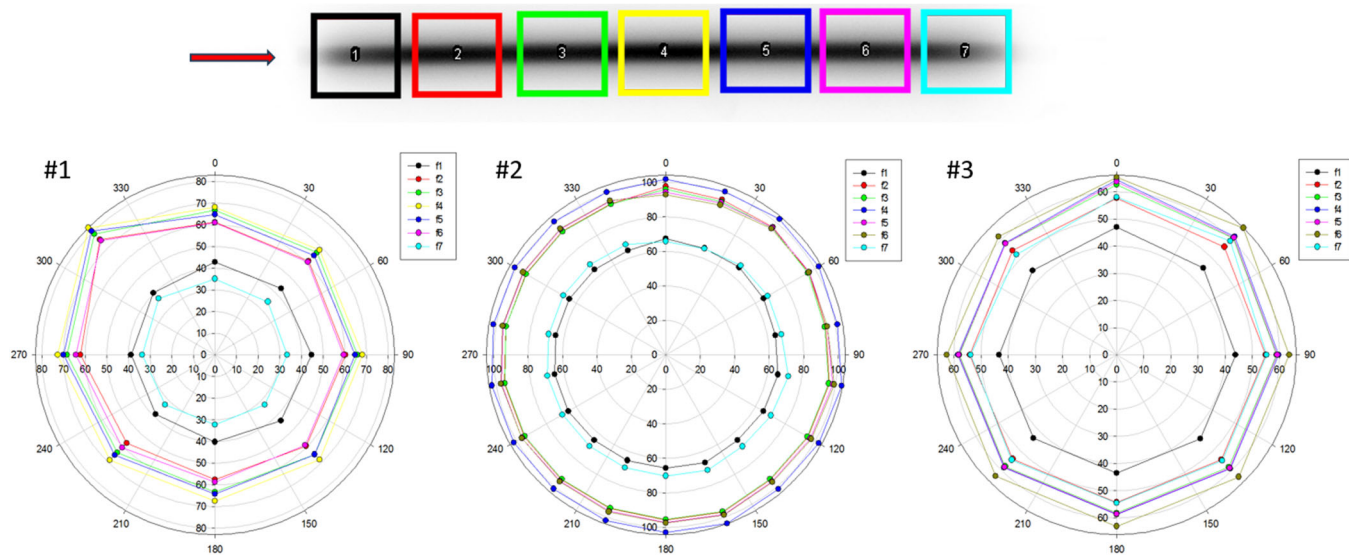


FIGURE 7 | Azimuth profiles of CDFs #1, #2 and #3 at seven positions along the diffuser tips as indicated in the intensity profile image on top (showing CDF #2).

the case for CDF #2. Also, the absolute values (bottom row in Figure 6) show interesting differences between the two types of fibers. For CDF #1, the addition of water strongly reduced the intensities, whereas only small changes were observed for CDF #2. In addition, the profile characteristic changed significantly for CDF #1, whereas it stayed identical for CDF #2.

3.1 | Azimuth Profiles

By manually turning the rotation mount with the CDF firmly fixed, multiple profile images can be recorded and evaluated. Figure 7 shows some examples. The best azimuth angle uniformity was recorded for CDF #2, while CDF #1 emits

considerably more light intensity to one side than to the opposite side.

4 | Discussion

The treatment effect of thermal or photodynamic light application is determined predominantly by the distribution of the light fluence rate in the target tissue and adjacent tissue. If CDFs are used for light transport and light application into the target volume, their light emission profiles should be known. This report proposes a simple, but still versatile measurement method to assess radial intensity profiles under realistic conditions and thus characterize the light emission characteristics of CDFs. The setup using a fluorescent layer can easily be implemented and provides a reliable intensity profile from a single shot image and multiple azimuth profiles from a series of images after rotation of the CDF. The fluorescence intensity profile is more reliable than a profile calculated from a directly taken image, because the fluorescent layer absorbs light emitted from the CDF surface in all polar angles equally. A direct image would only be able to detect light emitted from the CDF within angles, which hit the objective lens of the camera. If the polar angle distribution varies along the length of the diffuser tip, the resulting profile would be distorted. In contrast, the fluorescent layer serves as an isotropically sensitive light indicator and emits fluorescence strictly proportional to the absorbed fluence rate. As the fluorescence is emitted in all directions equally, the polar angles of the excitation light no longer influence the detected intensity. One should keep in mind, however, that in air, there will be an angle-and-polarization state dependent specular reflection of excitation light at the fluorescent layer's surface and less fluorescence will be induced for strongly forward or backward emitted excitation light. But, this is also true with tissue at the same location. In fact, the fluorescent layer can be regarded a thin slice of tissue, which reports the impinging light intensity (irradiance) to the camera. If the fluorescent layer is in contact with the CDF, the polar angle information is lost, but if at a given distance, any non-Lambertian emission from the CDF will produce axial shifts and distortions of the recorded profile, still correctly reporting the spatial distribution of the light emitted by the CDF on the "test-tissue."

In comparison to goniometer style measurement setups, such as used by Vesselov et al. [14], the fluorescent layer approach is much quicker as only one angular scanning is required instead of three (two angular and one longitudinal) scanning procedures to capture a full emission profile of the CDF. Furthermore, measurements in water are probably easier.

In air, all light, which leaves the diffusing rod of CDFs #1, #3, and #4 must have been scattered at a relatively large angle to not being reflected back into the rod by total internal reflection. Therefore, the direct image profile, which shows only light emitted perpendicularly, and the fluorescence image profile, which shows light at all angles equally, look quite similar (black and red lines in Figure 5).

In water, there is almost no total internal reflection at the diffusing rod boundary. Therefore, more light can leave the diffuser, but at angles, which cannot be detected by the camera as a direct image. The fluorescence image, however, shows this additional excitation light due to the isotropic distribution of

induced emission light from the fluorescent layer. This leads to a slight increase in the intensity recorded close to the proximal end of the diffuser tip (blue and red curves in the bottom left graph of Figure 6). Further down the rod, this light is lost compared to the situation in air and the recorded intensity decreases toward the distal end of the diffuser tip.

When looking at the fluorescence images recorded at 5 or 10 mm distance (lower two rows in Figure 4), one might be astonished by the fact that the diffuser tip is still visible as if directly imaged through the fluorescent layer. However, this can be attributed to the fluorescence light, which is emitted from the fluorescent layer toward the CDF and backscattered by the diffuser tip and then transmitted without further losses through the fluorescent layer and the longpass filters in front of the objective lens. The "white" diffuser tip of CDF #2 is therefore better visible than the more transparent diffuser tip of CDF #1. Interestingly, this does not significantly influence the real emission profile, as demonstrated by the similarity of the profiles calculated from the fluorescence images either including the diffuser tip (solid green and blue lines in Figure 5) or excluding it (dashed green and blue lines in Figure 5, see also bottom right image in Figure 4).

The setup can easily be immersed in water or other clear liquids. Changing the refractive index influences the profile significantly as shown in Figure 6. CDFs, which rely on a scattering rod with "volume scattering" (#1) may experience more changes than CDFs relying on a partial integrating sphere effect, which emit the light in a more Lambertian manner (#2).

This feasibility report focuses on establishing the described method for CDFs intended for use in PDT with a wavelength of 635 nm. It is not easy to find a fluorescent layer (glass or foil), which fluoresces at this excitation wavelength. Among the color glass filters of "RG" type available in the laboratory, it was only the RG695, which showed measurable fluorescence. But it served the purpose very well. It cannot be excluded that batch-to-batch variations of such color glass filters may have an influence on the fluorescence properties, as these are not part of the specifications. After completion of the measurements, we found an RG780 filter, which exhibited significantly more fluorescence than the RG695 filter employed in this report. Filters and foils with efficient fluorescence further in the visible are easily available. Further developments may employ NIR fluorochromes such as thulium-based nanocrystals [17] to build fluorescent layers with excitation wavelength ranges further in the infrared and potentially specified for the intended wavelength used.

There may be some concern that fluorescence may also be excited in the fiber, which might be imaged as a direct emission profile superimposed to the fluorescence image excited in the fluorescent layer. Although such fiber-induced internal fluorescence should be of the lowest intensity, its relative contribution to the imaged intensity profile can be estimated by inserting a short pass filter (transmitting excitation light but not fluorescence) between diffuser and fluorescent layer in the proposed measurement set-up. Such investigation should be performed when the proposed characterization technique is implemented in a standardized quality control process.

Fluorescence is not only emitted toward the camera, but also in “backwards” direction toward the diffuser tip. There it will be backscattered in “forward” direction toward the camera and may result in a reflection image of the diffuser tip (as shown in Figure 4, lower two rows). If this should strictly be avoided, one may equip the fluorescent layer with a shortpass coating. On the other hand, real tissue would also backscatter light and be influenced by the scatter characteristics of the diffuser tip—at least in the near field. Other profile measurement methods are also influenced by this effect, for example, a linear scan with an isotropic probe [16, 18].

Another limitation of the proposed method is the restriction in wavelengths. Only one wavelength at a time can be assessed and a suitable fluorescent layer has to be selected.

The spatial resolution one can obtain with this method depends on the absorption of the excitation wavelength in the fluorescent layer rather than on the resolution of the imaging optics and camera sensor. Therefore, one might think of improving the resolution by using very thin fluorescent layers. However, if these thin fluorescent layers transmit a considerable proportion of the excitation light, strongly forward or backward directed light would travel a longer distance within the fluorescent layer and then produce more fluorescence than perpendicularly emitted light. This would diminish the intriguing effect of the fluorescence technique to be emission angle independent.

An alternative approach might be to use a scattering layer instead of a fluorescent layer. Brief testing of this approach, however, showed that it is less reliable as there is multiple scatter between the layer and the diffuser tip, which itself artificially homogenizes local intensity inhomogeneity on the diffuser surface. As mentioned, with the fluorescence approach, the diffuser tip is also illuminated from backward directed fluorescence light, but there are no multiple scattering events. Although tissue will also backscatter light, the influence of this effect should be investigated and evaluated in artificial tissue phantoms with controlled optical properties.

The proposed simple method and set-up to characterize the radial light emission was intended to illustrate proof of principle. There are several improvements one may think of. Apart from the already mentioned shortpass coating of the fluorescent layer, hardware, and software could be automated, using motorized linear and rotation stages and synchronized one-click image acquisition and evaluation. Only 8 bits of the 12-bit dynamic range of the camera used in this setup were exploited for the purpose of this feasibility report. But, one might even extend the dynamic range by grabbing several images with controlled acquisition times and appropriate composition of the non-overexposed parts of each image. A size-optimized water container with an integrated fluorescent layer could enable measurements with tissue phantoms. Furthermore, the shape of the fluorescent layer might be changed, for example, to the shape of a hollow cylinder or to also measure light emitted from the diffuser tip in forward direction. For light dosimetry calculations, employing Monte Carlo or Raytracing algorithms, the 2D images from the fluorescent layer may serve as starting points for further

isotropic light propagation. If, in this context, the polar angle distribution along the diffuser tip is of interest, it may be retrieved from capturing fluorescent layer images at several known distances from the CDF.

5 | Conclusion

The detection of induced fluorescence instead of—or at least in addition to—direct emission to characterize CDF emission profiles enables a simple, fast, and reliable procedure. This approach allows for taking into account refraction-index mismatch by placing parts of the equipment into a suitable transparent liquid and container. It appears well suited for high throughput quality assurance measurements of CDFs. Based on this proof-of-principle description, a lot of improvements can be investigated and developed.

Author Contributions

Herbert Stepp: idea, conceptualization, measurements, data processing and presentation, critical discussion, manuscript draft. **Ronald Sroka:** conceptualization, critical discussion, manuscript review.

Acknowledgments

This report is dedicated to Dr. rer. nat. Reinhold Baumgartner, director of the LIFE Center at LMU Klinikum in Munich 1992–2010, who passed away November 24, 2020. Reinhold was initiator of many research projects in laser medicine and photodynamic medicine especially. He mentored dozens of young scientists, including medical doctors. His contributions to fluorescence guided surgery and PDT cover almost all medical disciplines. Establishing interstitial PDT with CDFs to treat malignant glioma was a main focus. Germany owes him the establishment of an internationally renowned center for photodynamic medicine. Open Access funding enabled and organized by Projekt DEAL.

Ethics Statement

The authors have nothing to report.

Consent

The authors have nothing to report.

Conflicts of Interest

The authors declare no conflicts of interest.

Data Availability Statement

Raw data can be made available upon justified request.

References

1. W. Beyer, “Systems for Light Application and Dosimetry in Photodynamic Therapy,” *Journal of Photochemistry and Photobiology B: Biology* 36, no. 2 (1996): 153–156.
2. L. Vesselov, W. Whittington, and L. Lilge, “Design and Performance of Thin Cylindrical Diffusers Created in Ge-Doped Multimode Optical Fibers,” *Applied Optics* 44, no. 14 (2005): 2754–2758.
3. L. Lilge, L. Vesselov, and W. Whittington, “Thin Cylindrical Diffusers in Multimode Ge-Doped Silica Fibers,” *Lasers in Surgery and Medicine* 36, no. 3 (2005): 245–251.

4. S. Ströbl, F. Wäger, M. Domke, A. Rühm, and R. Sroka, "Homogeneously Emitting, Mechanically Stable, and Efficient fs-Laser-Machined Fiber Diffusers for Medical Applications," *Lasers in Surgery and Medicine* 54, no. 4 (2022): 588–599.
5. M. A. Kosoglu, R. L. Hood, J. H. Rossmeisl Jr., et al., "Fiberoptic Microneedles: Novel Optical Diffusers for Interstitial Delivery of Therapeutic Light," *Lasers in Surgery and Medicine* 43, no. 9 (2011): 914–920.
6. A. Rendon, R. Weersink, and L. Lilge, "Towards Conformal Light Delivery Using Tailored Cylindrical Diffusers: Attainable Light Dose Distributions," *Physics in Medicine and Biology* 51, no. 23 (2006): 5967–5975.
7. G. A. Prasad, K. K. Wang, K. C. Halling, et al., "Utility of Biomarkers in Prediction of Response to Ablative Therapy in Barrett's Esophagus," *Gastroenterology* 135, no. 2 (2008): 370–379.
8. Y. Tan, S. Sun, D. Chen, et al., "Light Delivery Device Modelling for Homogenous Irradiation Distribution in Photodynamic Therapy of Non-Spherical Hollow Organs," *Photodiagnosis and Photodynamic Therapy* 34 (2021): 102320.
9. A. Johansson, F. Faber, G. Kniebühler, et al., "Protoporphyrinix-fluorescence and Photobleaching During Interstitial Photodynamic Therapy of Malignant Gliomas for Early Treatment Prognosis," *Lasers in Surgery and Medicine* 45, no. 4 (2013): 225–234.
10. A. Noweski, A. Roosen, S. Lebdai, et al., "Medium-Term Follow-Up of Vascular-Targeted Photodynamic Therapy of Localized Prostate Cancer Using TOOKAD Soluble WST-11 (Phase II Trials)," *European Urology Focus* 5, no. 6 (2019): 1022–1028.
11. P. M. Ripley, T. N. Mills, and J. A. S. Brookes, "Measurement of the Emission Profiles of Cylindrical Light Diffusers Using a Video Technique," *Lasers in Medical Science* 14, no. 1 (1999): 67–72.
12. S. Ströbl, M. Domke, A. Rühm, and R. Sroka, "Investigation of Non-Uniformly Emitting Optical Fiber Diffusers on the Light Distribution in Tissue," *Biomedical Optics Express* 11, no. 7 (2020): 3601–3617.
13. L. H. P. Murrer, J. P. A. Marijnissen, and W. M. Star, "Improvements in the Design of Linear Diffusers for Photodynamic Therapy," *Physics in Medicine and Biology* 42, no. 7 (1997): 1461–1464.
14. L. M. Vesselov, W. Whittington, and L. Lilge, "Performance Evaluation of Cylindrical Fiber Optic Light Diffusers for Biomedical Applications," *Lasers in Surgery and Medicine* 34, no. 4 (2004): 348–351.
15. A. Dimofte, J. C. Finlay, X. Liang, and T. C. Zhu, "Determination of Optical Properties in Heterogeneous Turbid Media Using a Cylindrical Diffusing Fiber," *Physics in Medicine and Biology* 57, no. 19 (2012): 6025–6046.
16. C. Dupont, G. Baert, S. Mordon, and M. Vermandel, "Parallelized Monte-Carlo Dosimetry Using Graphics Processing Units to Model Cylindrical Diffusers Used in Photodynamic Therapy: From Implementation to Validation," *Photodiagnosis and Photodynamic Therapy* 26 (2019): 351–360.
17. Y. Chang, H. Chen, X. Xie, et al., "Bright Tm(3+)-Based Downshifting Luminescence Nanoprobe Operating Around 1800 nm for NIR-IIb and c Bioimaging," *Nature Communications* 14, no. 1 (2023): 1079.
18. C. Munck, S. Mordon, and N. Betrouni, "Illumination Profile Characterization of a Light Device for the Dosimetry of Intra-Pleural Photodynamic Therapy for Mesothelioma," *Photodiagnosis and Photodynamic Therapy* 16 (2016): 23–26.